RSC Advances

PAPER

View Article Online
View Journal | View Issue

Check for updates

Cite this: *RSC Adv.*, 2023, **13**, 24767

$AlCl_3$@ZnO nanostructured material: an efficient green catalyst for the one-pot solvent-free synthesis of 1,4-dihydropyridines†

Santosh T. Shinde, *[a] Kaluram G. Kanade, *[a] Ramesh B. Gawade,[a] Vikram B. Hinge,[a] Manish D. Shinde,[b] Digambar B. Bankar,[c] Nitin M. Thorat[d] and Dinesh P. Amalnerkar[e]

$AlCl_3$-loaded ZnO nanoparticles have been explored as an efficient catalyst for 1,4-dihydropyridine synthesis under ambient temperature and solvent-free conditions. For this purpose, ZnO nanoparticles were synthesized by a simple solution-based precipitation technique using a stoichiometric amount of zinc sulfate and oxalic acid. The $AlCl_3$@ZnO nanocrystalline catalyst was prepared by loading 20% $AlCl_3$ on ZnO nanoparticles by a simple wet-impregnation technique. This catalyst efficiently performed Hantzsch pyridine reactions with various aromatic aldehydes, ethyl acetoacetate and ammonium acetate. The nanostructured $AlCl_3$-loaded ZnO catalyst was characterized by UV-DRS, XRD, FESEM, EDS, FETEM-STEM-EDS and XPS techniques. The comprehensive characterization reveals the formation of $AlCl_3$-loaded ZnO catalysts with an average particle size of 70–80 nm. The loading of $AlCl_3$ on the ZnO surface was confirmed by minor shifts in the XPS and XRD peaks. FETEM-STEM-EDS also indicates reasonable $AlCl_3$ loading on ZnO nanoparticles. The 20% $AlCl_3$-loaded ZnO nanocatalyst ($AlCl_3$@ZnO) confers 92% yield for the synthesis of 1,4-dihydropyridine under solvent-free and ambient temperature conditions. The synthesized 1,4-dihydropyridines were characterized by ^{1}H-NMR, ^{13}C-NMR, HRMS and FT-IR spectroscopic techniques. The reported catalyst is highly efficient, environmentally friendly and could become an alternative to homogenous and heterogenous catalytic reactions.

Received 26th June 2023
Accepted 29th July 2023

DOI: 10.1039/d3ra04277d

rsc.li/rsc-advances

Open Access Article. Published on 18 Avost 2023. Downloaded on 08/12/2025 08:13:16.
This article is licensed under a Creative Commons Attribution-NonCommercial 3.0 Unported Licence.

1. Introduction

Solving the recent challenge to obtain a high yield of Hantzsch pyridine synthesis using heterogeneous reactions has become an important task. Due to the significant biological activity of 1,4-dihydropyridines [1,4-DHPs] (Fig. 1), they belong to the important class of six-membered heterocyclic compounds.[1–3] The 1,4-DHP moiety occurs in many drugs and synthetic products.[4] The electron-withdrawing groups at 3 and 5 positions enhance the stability of 1,4-dihydropyridines.[5] Worldwide commercial representatives of DHPs such as nifedipine (Fig. 2A), amlodipine (Fig. 2B), felodipine (Fig. 2C) and nicardipine (Fig. 2D), are important drugs for the treatment of hypertension.[6,7] The 1,4-DHP skeletons have been used as an antimicrobial agent,[8–10] glycoprotein inhibitor,[11] calcium channel blocker,[12–18] anticancer agent,[19] and antitubercular agent.[20] Hantzsch diethyl 1,4-dihydro-2,6-dimethyl-3,5-pyridinedicarboxylate also acts as a good source of hydride for reduction purposes.[21–24] Therefore, the quest for cost-effective and simple methods for the synthesis of DHPs has become a hot topic of current research.

The traditional approach for the preparation of 1,4-dihydropyridines involved the condensation of three components,

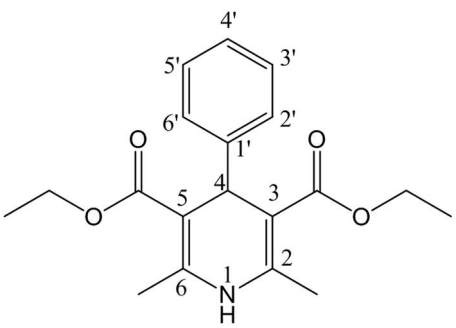

Fig. 1 The 1,4-dihydropyridine [1,4-DHP] moiety.

[a]Post Graduate Department of Chemistry and Research Centre, Annasaheb Awate College, Manchar-410503, India. E-mail: drsantoshinde@gmail.com
[b]Centre for Materials for Electronic Technology (C-MET), Off Pashan Road, Panchwati, Pune-411008, India
[c]Post Graduate Department of Chemistry and Research Centre, R. B. Narayanrao Borawake College, Shrirampur-413709, India
[d]Post Graduate Department of Chemistry and Research Centre, Maharaja Jivajirao Shinde Mahavidyalaya, Shrigonda, Ahmednagar-413701, India
[e]Department of Technology, Savitribai Phule Pune University, Pune-411007, India

† Electronic supplementary information (ESI) available. See DOI: https://doi.org/10.1039/d3ra04277d

© 2023 The Author(s). Published by the Royal Society of Chemistry

Open Access Article. Published on 18 Avost 2023. Downloaded on 08/12/2025 08:13:16.
This article is licensed under a Creative Commons Attribution-NonCommercial 3.0 Unported Licence.

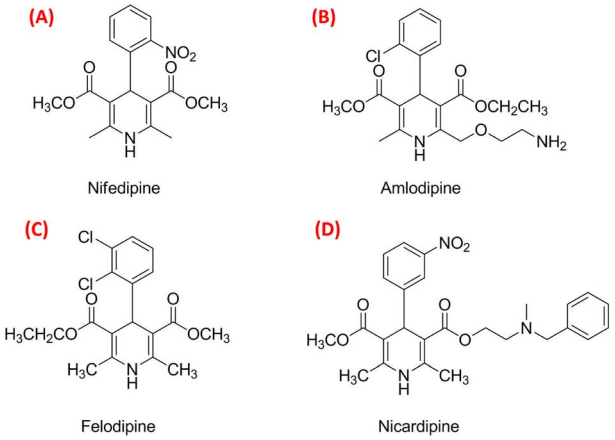

Fig. 2 The best-selling drugs nifedipine (A), amlodipine (B), felodipine (C) and nicardipine (D) that are used in the treatment of hypertension.

viz. aromatic aldehyde, β-keto ester and ammonia, *via* acid-catalyzed organic reactions. The familiar reaction was performed under acid-catalyzed conditions, such as melamine trisulfonic acid,[25] phenylboronic acid[26] or *p*-toluenesulfonic acid.[27] Hantzsch pyridine synthesis has been also performed in the presence of Lewis acid catalysts such as Zn[(L)proline]$_2$,[28] Aluminium(III) chloride hexahydrate[29] and $ZnCl_2$.[30] However, the recyclability of Lewis acid and homogenous organic acid catalysts has become an environmental concern.

To overcome the recyclability of catalysts and environmental issues, the reactions were performed by biodegradable catalysis[31] and heterogeneous catalysis using clay,[32] ZnO,[33] Cu–ZnO,[34] CaO,[35] N-doped TiO_2,[36] V_2O_5/ZrO_2,[37] Fe_3O_4 [38] or CuO/rGO.[39] The comparative features of organic transformations with respect to catalytic conditions are given in Table 1.

However, these reactions are time consuming and need solvents and high temperature, microwave assistance as well as tedious workup procedures. In order to overcome these limitations 1,4-dihydropyridines was recently synthesized in high yield by a green approach using an acidic functional group loaded on nanocrystalline metal oxides.[40] Therefore, as a part of ongoing exploration related to the development of a clean and eco-friendly method, herein we report an environmentally friendly $AlCl_3$-loaded ZnO nanostructured catalyst for the synthesis of 1,4-dihydropyridine.

We report that the use of $AlCl_3$-loaded ZnO nanostructured catalysts not only enhances the yield, but also turns out to be cost effective for the synthesis of 1,4-dihydropyridine. For this purpose, a vital $AlCl_3$@ZnO nanocatalyst was synthesized using a simple solution-based wet-impregnation technique,[41,42] as described in the following experimental section. Notably, our nanocrystalline $AlCl_3$@ZnO material was found not only to be an efficient catalyst but also helps to obtain highly pure 1,4-dihydropyridine derivatives at room temperature under solvent-free conditions.

2. Experimental

2.1. Synthesis of nanocrystalline ZnO

For the synthesis of ZnO nanoparticles, oxalic acid (99.9%, SD-fine chemicals) and zinc sulfate (99.9%, SD-fine chemicals) were used as precursors. To begin with, the oxalic acid (0.1 N) solution was added dropwise into the zinc sulfate solution (0.1 N) with constant stirring until the formation of a zinc oxalate complex. The obtained precipitate of zinc oxalate complex was washed with distilled water and dried at 100 °C in an oven. Then this intermediate complex was decomposed at 500 °C for 5 h in order to obtain nanocrystalline zinc oxide.

2.2. Synthesis of nanostructured $AlCl_3$@ZnO

For the synthesis of nanostructured $AlCl_3$@ZnO, as-synthesized nanocrystalline ZnO was used as a precursor material. The appropriate amounts of nanocrystalline ZnO (80%) and $AlCl_3$ (20%) were mixed in a mortar and pestle and subsequently transferred to a round-bottom flask (500 mL) containing 100 mL of *n*-hexane. The reaction mass was further refluxed for 2 h and excess solvent was removed by vacuum distillation and the resultant solid was dried at 100 °C for 4 h to obtain nanocrystalline $AlCl_3$@ZnO material.

Table 1 Literature survey on biodegradable catalysis and heterogeneous catalysis

Target molecule	Reaction conditions	Yield[a] (%)
2*H*-Indazolo[1,2-β] phthalazine-triones	PEG-OSO_3H, solvent-free, 80 °C	80–93 (ref. 31)
Tetrahydroquinolines	Montmorillonite KSF, water, refluxing conditions, 48 h	87–95 (ref. 32)
3,4-Dihydropyrimidin-2(1*H*)-ones/thiones	ZnO NPs, MW, solvent free, 55 °C	60–75 (ref. 33)
(*E*)-3-Styrylchromones	Cu–ZnO NPs, DMF, reflux conditions	68–80 (ref. 34)
2-Amino-3,5-dicyano-6-sulfanyl pyridines	Nano-CaO, ethanol:water (1 : 1), 50 °C	75–92 (ref. 35)
Diethyl(1-phenyl-3-(thiophene-2-yl)-1*H*-pyrazole-4-yl) (phenylamino) methylphosphonates	N-Doped TiO_2, microwave irradiation for 10–15 min using 420 W	71–95 (ref. 36)
1,4-Dihydropyridine	V_2O_5/ZrO_2 ethanol, RT, 15 min	90–96 (ref. 37)
Pyrazolophthalazinyl spirooxindoles	Fe_3O_4\SiO_2\methylene dipyridine MNPs, RT, solvent-free	90–93 (ref. 38)
Imidazo[1,2-α]pyridines	Cu(0)/rGO, ultrasonicated for 2 min, stirring at 110 °C for 8 h	84–96 (ref. 39)

[a] The comparative features of biodegradable and heterogeneous catalysis for organic transformations.

© 2023 The Author(s). Published by the Royal Society of Chemistry

Open Access Article. Published on 18 Avost 2023. Downloaded on 08/12/2025 08:13:16.
This article is licensed under a Creative Commons Attribution-NonCommercial 3.0 Unported Licence.

2.3. Characterization of powdered ZnO and $AlCl_3$@ZnO catalyst

To determine the crystal structure and phase purity of the resultant nanomaterials, X-ray diffractograms (XRD) of the samples were obtained with a Rigaku-D8/MaX-2200V using Ni-filtered Cu-Kα radiation ($\lambda = 1.54$ Å). The surface morphological features along with particle size were determined with a field emission scanning electron microscope (FESEM; HITACHI S-4800 and Nova Nano SEM NPEP303). For this purpose, the powder sample was drop-cast on conducting carbon tape attached to an aluminium stub and the resultant layer was subsequently coated with conducting gold film to minimize the effects due to charging. The FESEM measurements were carried out at an accelerating voltage of 20 kV, working distance of ~10.2 mm and using secondary electron detector mode. Fine-scale microstructural evaluation of the synthesized ZnO sample was carried out by obtaining field emission transmission electron microscopic (FETEM) images using a JEOL-2200EX instrument. This instrument was also employed for energy dispersive spectroscopy (EDS) and associated elemental mapping studies in scanning transmission electron microscopy (STEM) configuration with bright field mode. The UV-Visible diffuse-reflectance spectra (UV Vis-DRS) were recorded using a UV-Vis diffuse-reflectance spectrophotometer (PerkinElmer, model: Lambda 365). To find the electronic states of the elements in the nanocrystalline $AlCl_3$@ZnO material, X-ray photoelectron spectroscopic (XPS) scans were acquired with a Thermo Fisher Scientific instrument, UK (Model K ALPHA+). The X-ray source used during the analysis was Al K alpha (monochromatic) with 6 mA beam current and the spot size on the samples was 400 micrometres. All the XPS spectra were corrected using the adventitious C 1s peak at 284.8 eV.

The progress of the reaction was monitored by the thin layer chromatography (TLC) technique. The ^{1}H NMR and ^{13}C NMR spectra of the Hantzsch reaction products were recorded on a Bruker Ascend 500 NMR spectrometer operating at 500 MHz and 125 MHz, respectively, in $CDCl_3$ solvent. The ^{1}H and ^{13}C chemical shifts (δ) are reported in ppm relative to tetramethylsilane (TMS), as the internal standard substance. The coupling constant (J) values are expressed in Hz. A high-resolution mass spectrometer (Bruker Germany, model: Impact HD, UHR Impact II ESI-Q-TOF) was used for mass analysis of product materials in methanol solvent. The FT-IR spectra were acquired on a Shimadzu FT-IR Affinity 1S.

2.4. Measurement of catalytic activity for Hantzsch pyridine synthesis

Stoichiometric amounts of aromatic aldehydes (4.71 mmol), ethyl acetoacetate (9.42 mmol) and ammonium acetate (5.66 mmol) were taken in a 25 mL round-bottom flask (Scheme 2). Then, nanocrystalline $AlCl_3$@ZnO (1.17 mmol) powder was added as a catalyst in the reaction mixture, which was stirred for 2 h at room temperature. The reaction was monitored by TLC. After completion of the reaction, 10 mL of chloroform was added to the reaction mass in order to separate the product. The catalyst was separated by the centrifugation technique. Subsequently, the filtrate was concentrated to get a solidified compound and then crystallized in diethyl ether to get a pure product. The structural purity of the compounds was confirmed by FT-IR, ^{1}H NMR, ^{13}C NMR and HRMS spectral techniques.

3. Results and discussion

3.1. XRD study of pure ZnO and $AlCl_3$@ZnO

Fig. 3(a–e) furnish XRD patterns of pure ZnO, 5%, 10%, 15% and 20% $AlCl_3$@ZnO, respectively. The peaks appearing in the XRD patterns disclosed the wurtzite hexagonal form of ZnO (JCPDS card: 89-1397). The orientation of the peak at the (002) plane indicates the polycrystalline nature; other XRD peaks corresponding to (100), (101), (102), (110), (103) and (112) planes are in good agreement with the standard data.

Fig. 4 shows small shifts in diffraction angle (2θ) corresponding to (100), (101) and (102) peaks due to the $AlCl_3$ loading in ZnO.[44,45] The relative intensities of the peaks corresponding to the (002) plane of pure ZnO and $AlCl_3$-loaded ZnO imply an increase in crystal size. The XRD reveals only ZnO peaks and no peaks related to aluminium chloride (and its components) are observed. A plausible reason may be the dominance of an amorphous state of aluminium chloride dispersed uniformly on ZnO NPs, so it may be very hard to detect by XRD.

The average crystallite sizes of pure ZnO, 5%, 10%, 15% and 20% $AlCl_3$-loaded ZnO samples were calculated using Scherrer's equation and were found to be 22.41, 28.61, 32.58, 32.98 and 33.62 nm, respectively. The slight increase in crystallite size may be due to loading of $AlCl_3$ on ZnO.

3.2. UV-Vis diffuse reflectance spectroscopy (DRS) of ZnO and $AlCl_3$@ZnO

Fig. 5 shows the UV-Vis (DRS) absorption spectra of pure ZnO and $AlCl_3$@ZnO NPs measured in the range of 200–800 nm. In the absorption spectra, the optical absorption edge in the UV region appears to shift slightly to the higher wavelength region

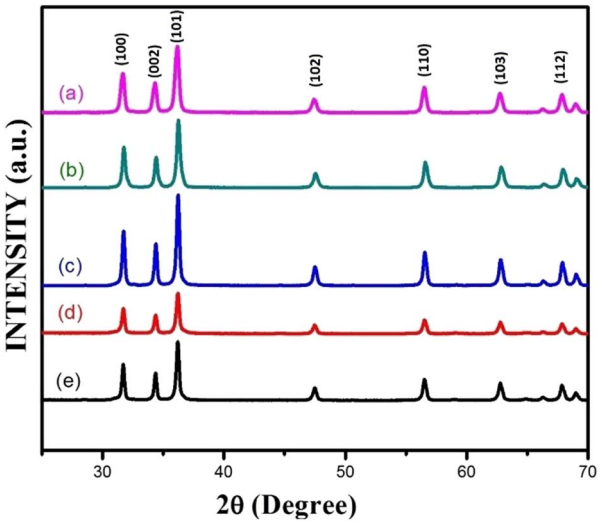

Fig. 3 X-ray diffraction patterns of (a) as-synthesized pure ZnO powder and $AlCl_3$@ZnO powders corresponding to wt% loadings of (b) 5%, (c) 10%, (d) 15%, and (e) 20%.

Open Access Article. Published on 18 Avost 2023. Downloaded on 08/12/2025 08:13:16.
This article is licensed under a Creative Commons Attribution-NonCommercial 3.0 Unported Licence.

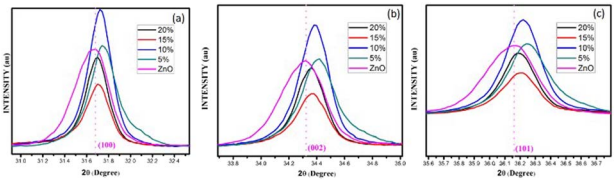

Fig. 4 The shifts in peak position in the X-ray diffraction angles corresponding to (a) (100), (b) (002) and (c) (101) planes for as-synthesized pure ZnO powder and $AlCl_3$@ZnO powders corresponding to wt% loadings of 5%, 10%, 15%, and 20%.

(red shift) with an increase in $AlCl_3$-loading concentration (Table 2).

At higher energy, the transformation of the relatively flat UV-DRS absorption curve for pure nanocrystalline ZnO to increasingly bent ones indicates a subsequent increase in loading of $AlCl_3$. However, broad UV emission is observed for $AlCl_3$-loaded ZnO.

Fig. 6(a–e) present the Tauc plots for pure ZnO and $AlCl_3$-loaded ZnO NPs. The optical energy band gap is calculated using the formula

$$(\alpha\eta\nu)^2 = \beta(h\nu - E_g) \quad (1)$$

where α = absorption coefficient, β = a constant (generally known as the band tailing parameter), $h\nu$ = photon energy, E_g = optical band gap energy and 'n' is an index which may take values of 1/3, 1/2, 2, or 3, depending upon the type of band-to-band transition.

The band gaps of each synthesized catalyst material were calculated using the above equation by considering $n = 2$, the case for a direct band gap transition (Fig. 6(a–e)).

The band gap values calculated for pure ZnO and 5%, 10%, 15% and 20 weight % $AlCl_3$-loaded ZnO NPs presented in Table 2 disclose that, as the concentration of $AlCl_3$ increases in ZnO,

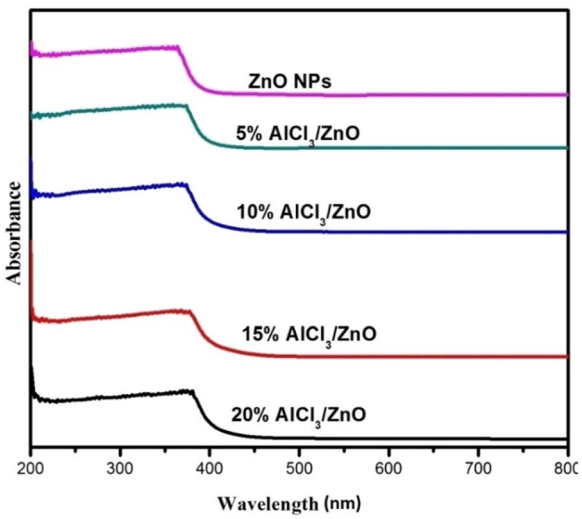

Fig. 5 UV-Vis DRS spectra of as-synthesized pure ZnO NPs, 5% $AlCl_3$@ZnO NPs, 10% $AlCl_3$@ZnO NPs, 15% $AlCl_3$@ZnO NPs and 20% $AlCl_3$@ZnO NPs.

Table 2 Cut-off wavelength and band gap energy of pure ZnO and $AlCl_3$-loaded ZnO samples

Sr. No.	Catalyst	Cut-off wavelength (nm)	Band gap (eV)
1	ZnO	383.75	3.127
2	5% $AlCl_3$@ZnO	385.10	3.116
3	10% $AlCl_3$@ZnO	387.22	3.099
4	15% $AlCl_3$@ZnO	389.86	3.078
5	20% $AlCl_3$@ZnO	416.85	3.059

a continuous decrease in band gap is noticed, which is consistent with the XRD data of a slight increase in grain size with $AlCl_3$ loading.[43]

3.3. Morphology study of ZnO and $AlCl_3$@ZnO by FESEM

The FESEM images of ZnO and $AlCl_3$@ZnO nanomaterials are displayed in Fig. 7. Fig. 7(a and b) show images of nanocrystalline ZnO material at 1 μm and 200 nm scale, which portray the formation of pallet-shaped nano-scale ZnO particles of size 40–80 nm (width-wise) and 80–200 nm (length-wise). Fig. 7(c, d), (e, f), (g, h) and (i, j) are the FESEM images of 5% $AlCl_3$@ZnO, 10% $AlCl_3$@ZnO, 15% $AlCl_3$@ZnO and 20% $AlCl_3$@ZnO, respectively, at the 1 μm and 200 nm resolution. The high-resolution image shows the formation of a flower-like morphology with adjacent spherical shaped particles of size 70–100 nm in some cases.

3.4. Characterization by FETEM

The representative TEM images of as-synthesized nanocrystalline ZnO samples (Fig. 8(a–c)) show predominantly nanorod morphology along with other shapes having faceted growth and having particle sizes in the range of 80–200 nm for length and 40–100 nm for width. The overall size calculated by TEM study is in good agreement with the FESEM study. The average d-spacing as observed from the HRTEM image (Fig. 8(e)) is 0.267 nm, which typically corresponds to the (002) plane of ZnO, hinting at the localized single crystalline lattice pattern of ZnO nanoparticles. The selected area electron diffraction pattern (SAED) shown in Fig. 8(f) reveals bright spots aligned in a particular direction which

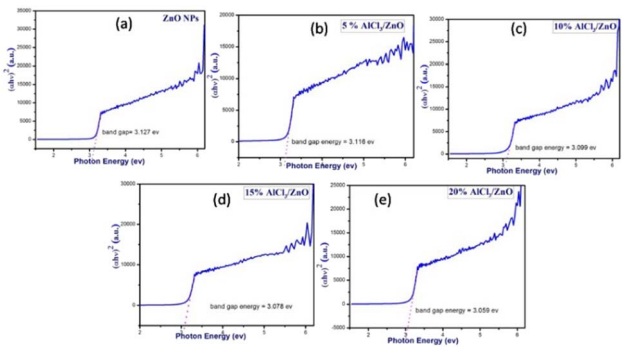

Fig. 6 Tauc plots of (a) as-synthesized pure ZnO NPs and $AlCl_3$@ZnO NPs corresponding to wt% loadings of (b) 5%, (c) 10%, (d) 15%, and (e) 20%.

© 2023 The Author(s). Published by the Royal Society of Chemistry

Open Access Article. Published on 18 Avost 2023. Downloaded on 08/12/2025 08:13:16.
This article is licensed under a Creative Commons Attribution-NonCommercial 3.0 Unported Licence.

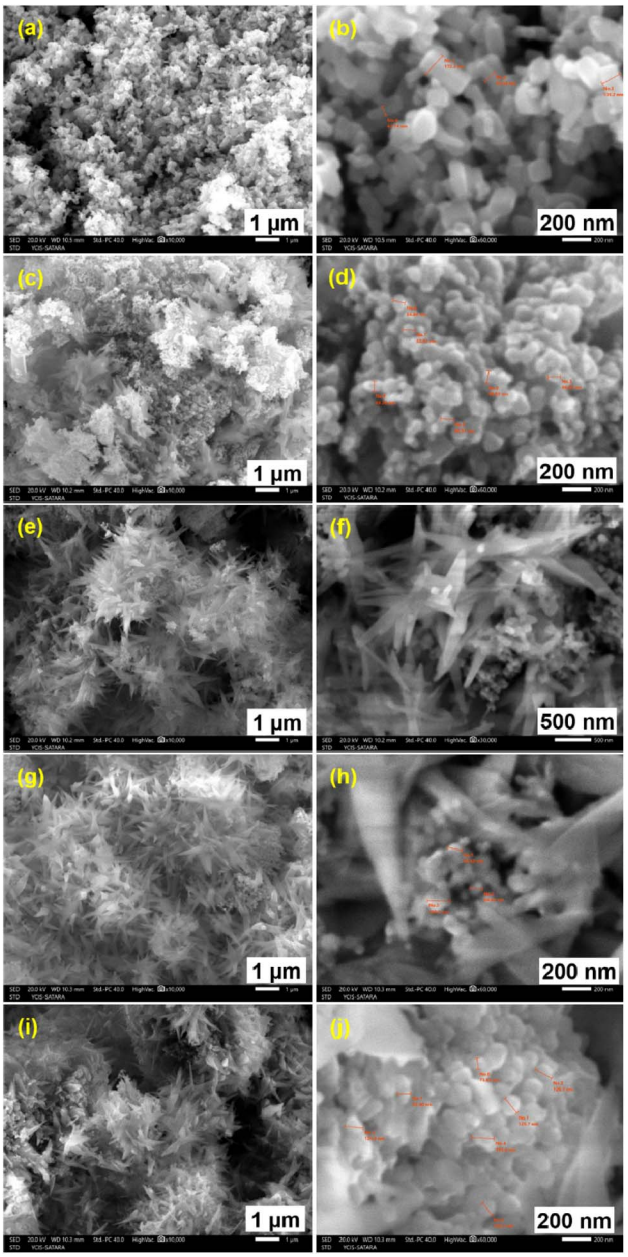

Fig. 7 FESEM images of ZnO (a and b), 5% $AlCl_3$@ZnO (c and d), 10% $AlCl_3$@ZnO (e and f), 15% $AlCl_3$@ZnO (g and h), 20% $AlCl_3$@ZnO (i and j).

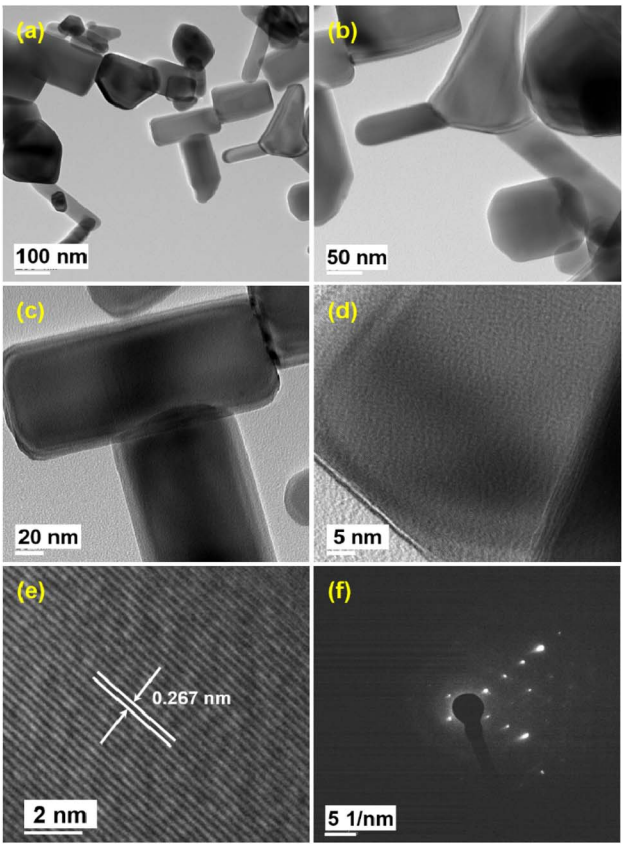

Fig. 8 FETEM images of ZnO nanomaterials at (a–c) low, (d) intermediate, and (e) high magnification and (f) corresponding SAED pattern.

also substantiates the localized single crystalline nature of ZnO nanoparticles.[46]

3.5. FETEM-STEM-EDS analysis of $AlCl_3$-loaded ZnO nanostructure

Energy dispersive X-ray spectroscopy (EDS) analysis was used for validation and quantification of the elements present in the given sample *via* scanning transmission electron microscopy (STEM) mode. In our investigation, weight-by-weight amounts of $AlCl_3$ and ZnO were used in the wet impregnation method. For FETEM-STEM-EDS elemental composition analysis, we considered the 20% $AlCl_3$@ZnO sample, and the associated qualitative elemental mapping as well as quantitative EDS data are reproduced in Fig. 9. The EDS-elemental mapping images of the 20% $AlCl_3$@ZnO sample taken in STEM mode are shown in Fig. 9. The elemental mapping images due to Zn and O (Fig. 9(b and c), respectively) overlap well with the corresponding electron image (Fig. 9(a)). The intensity of the colours assigned to Zn and O is also very high. The elemental mapping images for Al and Cl (Fig. 9(d and e), respectively) also overlap with the corresponding electron image; however, the intensity of the colours attributable to these two elements is low, which is obvious as only 20 wt% $AlCl_3$ is used for the purpose of surface loading. The FETEM results are in agreement with the FESEM results, which comprehensively confirms the surface loading of $AlCl_3$ over ZnO nanoparticles.

For quantitative FETEM-STEM-EDS composition analysis, the relevant EDS spectrum and elemental composition data (in tabular form) are reproduced in Fig. 9. The EDS spectrum discloses that the 20% $AlCl_3$@ZnO nanomaterial contains 24.73 wt% of oxygen, 7.74 wt% of chlorine, 41.16 wt% of zinc and 9.01 wt% of aluminium, even though the XRD pattern did not show any peaks of aluminium and/or its compounds. The EDS spectrum also reveals that the 20% $AlCl_3$@ZnO contains 9.36 atomic% of Al and 10.55 atomic% of Cl. Overall, EDS (qualitative and quantitative) analysis has revealed that the sample is composed of Zn, O, Al and Cl, which is in good agreement with results obtained by XPS (Fig. 10).

Open Access Article. Published on 18 Avost 2023. Downloaded on 08/12/2025 08:13:16.
This article is licensed under a Creative Commons Attribution-NonCommercial 3.0 Unported Licence.

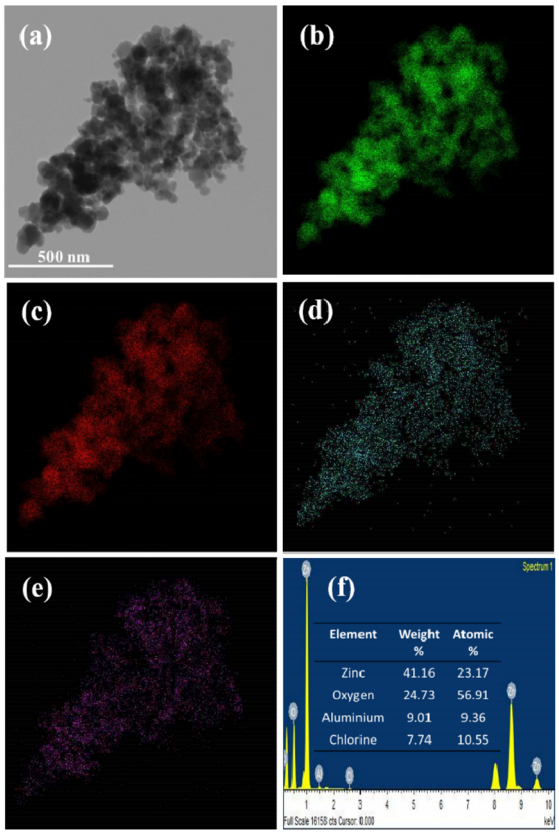

Fig. 9 FETEM-STEM-EDS elemental mapping images of the 20% $AlCl_3$@ZnO catalyst corresponding to (a) electron image, and elemental mapping images corresponding to (b) Zn, (c) O, (d) Al and (e) Cl and (f) STEM-EDS spectrum exhibiting quantitative elemental composition data for nanostructured 20% $AlCl_3$@ZnO.

3.6. XPS study of $AlCl_3$-loaded ZnO nanomaterials

X-ray photoelectron spectroscopy (XPS) detects the elemental composition and chemical state of an element. Fig. 10 shows the XPS spectrum of an $AlCl_3$@ZnO material used to study the surface exposure of ZnO and their respective additives, and their chemical states.

The high-resolution XPS spectra of nanostructured $AlCl_3$@ZnO mainly confirmed the existence of Zn 2p, Al 2p, O 1s and Cl 2p elements in the sample. The Zn 2p peaks appearing at 1021.6 eV and 1044.7 eV are related to Zn $2p_{3/2}$ and Zn $2p_{1/2}$, which are the characteristic features of Zn^{2+} in Zn(II)O. The two O 1s peaks belong to the lattice (O^{2-}) oxide sites (530.3 eV) and the Zn(II)–OH groups of oxygen (531.5 eV). The binding energy peaks at 74.4 eV and 74.7 eV signify the Al $2p_{3/2}$ and Al $2p_{1/2}$ energy states, respectively. This binding energy values can be assigned to Al^{3+} species in Al_2O_3 [47] and $AlCl_3$,[48] respectively. The binding energy at 199.58 eV denotes the Cl $2p_{3/2}$ energy state of metal chloride.[49] The overall appearance of peaks in XPS scans demonstrates the successful loading of $AlCl_3$ on the surface of ZnO nanoparticles.

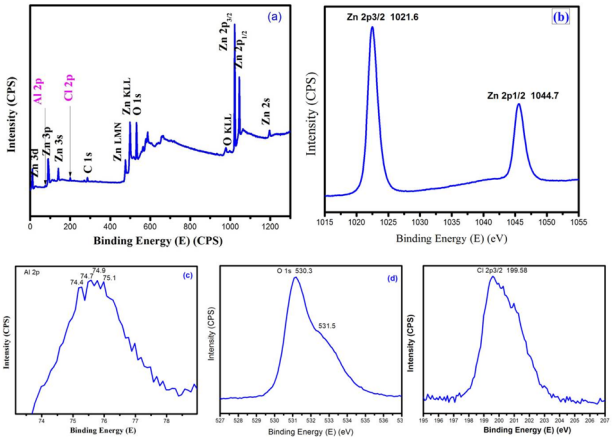

Fig. 10 X-ray photoelectron spectra of $AlCl_3$/ZnO (a) survey spectrum, (b) Zn 2p, (c) Al 2p, (d) O 1s and (e) Cl 2p.

3.7. Measurement of catalytic activity of $AlCl_3$-loaded ZnO NPs for Hantzsch pyridine synthesis

In the present protocol, we began with the optimization of reaction conditions for the synthesis of dihydropyridines. We took 0.5 g of benzaldehyde, 1.22 g of ethyl acetoacetate and 0.43 g of ammonium acetate as starting materials for the model reaction (Scheme 1). The reaction was performed at room temperature under solvent-free conditions.

3.7.1. Catalytic study for the synthesis of 1,4-dihydropyridine. One-pot synthesis of 1,4-dihydropyridine was carried out without using any catalyst, which led to the formation of a trace amount of product in 4 h (Table 3, entry 1), thus pointing out the necessity of a suitable catalyst in such a reaction.

Then the feasibility of the reaction was checked with different catalysts, such as ZnO NPs, anhydrous $AlCl_3$, 5% $AlCl_3$@ZnO NPs, 10% $AlCl_3$@ZnO NPs, 15% $AlCl_3$@ZnO NPs, and 20% $AlCl_3$@ZnO NPs (Table 3, entries 2–7). $AlCl_3$ works as a Lewis acid catalyst with comparative yield to ZnO. The yield of 1,4-dihydropyridine increases after the use of $AlCl_3$@ZnO NPs. The results demonstrated that the yield of 1,4-dihydropyridine increases as the loading % of $AlCl_3$ increases in the ZnO nanocatalyst (Table 3, entries 4–7).

It was observed that the 20% $AlCl_3$@ZnO nanocatalyst is more efficient for the synthesis of 2,6-dimethyl-4-phenyl-1,4-dihydropyridine-3,5-diethylcarboxylate (Table 3, entry 7). It disclosed up to 94% conversion into the product. The enhancement of yield could be due to the availability of more active space on the catalyst, as observed in the FESEM and XPS studies.

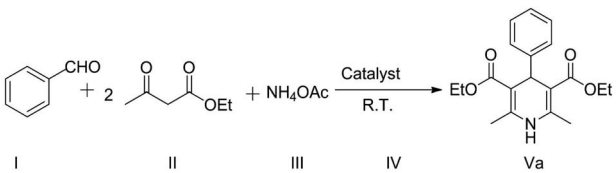

Scheme 1

© 2023 The Author(s). Published by the Royal Society of Chemistry

Open Access Article. Published on 18 Avost 2023. Downloaded on 08/12/2025 08:13:16.
This article is licensed under a Creative Commons Attribution-NonCommercial 3.0 Unported Licence.

Table 3 Preparation of 1,4-dihydropyridine under different catalytic and solvent-free conditions[a]

Entry	Catalyst	Time (h)	Yield[b]
1	—	4	Trace
2	ZnO	2	54
3	Anhydrous $AlCl_3$	2	60
4	5% $AlCl_3$@ZnO NPs	2	70
5	10% $AlCl_3$@ZnO NPs	2	74
6	15% $AlCl_3$@ZnO NPs	2	83
7	20% $AlCl_3$@ZnO NPs	2	94

[a] Reaction conditions: benzaldehyde (4.71 mmol), ethyl acetoacetate (9.42 mmol), ammonium acetate (5.66 mmol), and catalyst (4.71 mmol, 1 equiv.), room temperature. [b] Isolated yield.

3.7.2. Optimization of reaction in different mole equivalents of $AlCl_3$@ZnO nanocatalyst for the synthesis of 1,4-dihydropyridine. By using model reaction 1, we checked the feasibility of the reaction for different mole equivalent quantities of the catalyst at room temperature and under solvent-free conditions. The obtained results are furnished in Table 4, entries 1–7.

It was found that 20% $AlCl_3$@ZnO gives up to 92% conversion of reactant into product using 0.25 mol equiv. of catalyst (Table 4, entry 6).

3.7.3. Effect of solvents on the synthesis of 1,4-dihydropyridine. We also investigated the effect of solvent on the synthesis of 1,4-dihydropyridine (Va) at ambient temperature (Table 5, entries 1–10) for the model reaction. We observed that water solvent is not suitable for conversion. Methanol, ethanol and acetonitrile are suitable to obtain yields of around 80–84% (Table 5, entries 2–4).

Among the various solvents, the solvent-free condition is more suitable for the synthesis of 1,4-dihydropyridine using 0.25 mol equiv. of 20% $AlCl_3$@ZnO catalyst at room temperature. Under solvent-free conditions, we obtained 92% yield for the model reaction (Table 5, entry 11).

3.7.4. Synthesis of substituted 1,4-dihydropyridine using 20% $AlCl_3$-loaded ZnO. After optimization of reaction conditions, we found that solvent-free, room temperature and 0.25 mol equiv. of 20% $AlCl_3$-loaded ZnO catalytic conditions are more suitable for the synthesis of 1,4-dihydropyridine. Therefore, we used the same parameters for the synthesis of differently substituted 1,4-dihydropyridines, which is shown in Scheme 2 and the observed yields are provided in Table 6.

The effect of electron donating and withdrawing substitution on aromatic aldehyde at the o/p position has been studied for the synthesis of 1,4-dihydropyridines (4a–4n) under solvent-free conditions and 0.25 mol. equiv. of 20% $AlCl_3$@ZnO NPs at ambient temperature (Table 6, entries 1–14). The presence of an electron donating OH (p) group on aromatic aldehyde reduces the yield of reaction (Table 6, entry 8). Halogenated aromatic aldehydes (Table 6, entries 3–4 and 10–12) gave a better yield. For nitrobenzaldehyde the obtained yields are 80% and 75% (Table 6, entries 6–7). Benzaldehyde, 4-chlorobenzaldehyde and 4-methoxybenzaldehyde gave the best yields (Table 6, entries 1, 2 and 5). The formation of 1,4-dihydropyridines were confirmed ^{1}H-NMR, ^{13}C-NMR, HRMS and FT-IR spectral data (please see ESI†).

3.7.5. Proposed mechanism for the synthesis of 1,4-dihydropyridine derivatives. Worldwide, the synthesis of Hantzsch pyridine has been carried out using organic acids and Lewis acids as catalysts under refluxing conditions. The catalytic activity of nanocrystalline metal oxide has been enhanced by loading/doping those materials with an acidic moiety. We have developed an environmentally friendly $AlCl_3$-loaded ZnO nanostructured catalyst for the synthesis of 1,4-dihydropyridine. $AlCl_3$ is a well-known Lewis acid catalyst with a tendency to accept a lone pair of electrons. We observed that the catalytic activity of $AlCl_3$@ZnO has been enhanced for the proposed reaction. The proposed Hantzsch reaction is the three-component condensation of aromatic aldehyde (1 equiv.), ethyl acetoacetate (2 equiv.) and ammonium acetate (1 equiv.). Ethyl acetoacetate is an electron-rich species with a tendency to donate the lone pair of electrons present in oxygen. It can react with more reactive $AlCl_3$@ZnO, forming an intermediate enolate (as outlined in the proposed mechanism). Subsequently, $AlCl_3$@ZnO makes aromatic aldehyde more electron deficient by withdrawing an electron from the carbonyl group and, in

Table 4 Preparation of 1,4-dihydropyridine under different mole equivalent quantities of 20% $AlCl_3$@ZnO catalyst at ambient temperature[a]

Entry	Amount of catalyst (mol equiv.)	Time (h)	Yield[b]
1	—	4	Trace
2	0.05	2	60
3	0.10	2	72
4	0.15	2	82
5	0.20	2	87
6	0.25	2	92
7	0.30	2	92

[a] Reaction conditions: benzaldehyde (4.71 mmol), ethyl acetoacetate (9.42 mmol), ammonium acetate (5.66 mmol), and catalyst (20%), under solvent-free conditions, room temperature. [b] Isolated yield.

Table 5 Effect of solvents for the synthesis of 1,4-dihydropyridine at ambient temperature using 20% AlCl@ZnO catalyst[a]

Entry	Solvent	Time (h)	Yield[b]
1	H_2O	6	Trace
2	Methanol	2	80
3	Ethanol	2	84
4	THF	2	70
5	Acetonitrile	2	80
6	Acetone	2	78
7	CH_2Cl_2	2	70
9	Toluene	2	60
10	DMF	2	68
11	Solvent-free	2	92

[a] Reaction conditions: benzaldehyde (4.71 mmol), ethyl acetoacetate (9.42 mmol), ammonium acetate (5.66 mmol), and catalyst (1.17 mmol, 0.25 equiv.) in different solvent conditions. [b] Isolated yield.

© 2023 The Author(s). Published by the Royal Society of Chemistry

Open Access Article. Published on 18 Avost 2023. Downloaded on 08/12/2025 08:13:16.
This article is licensed under a Creative Commons Attribution-NonCommercial 3.0 Unported Licence.

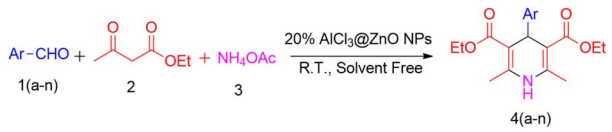

Scheme 2

Table 6 Synthesis of 1,4-dihydropyridines (4a–n) using 20% $AlCl_3$@ZnO catalyst under solvent-free conditions[a]

Entry	Ar 1(a–n)	Compound 4(a–n)	Yield[b]
1	C_6H_5	4a	92
2	4-ClC_6H_4	4b	93
3	4-FC_6H_4	4c	90
4	4-BrC_6H_4	4d	88
5	4-$OMeC_6H_4$	4e	92
6	4-$NO_2C_6H_4$	4f	80
7	2-$NO_2C_6H_4$	4g	75
8	4-OHC_6H_4	4h	78
9	2-Cl, 6-FC_6H_3	4i	78
10	2-ClC_6H_4	4J	86
11	3-ClC_6H_4	4k	88
12	2-FC_6H_4	4l	88
13	4-$CH_3C_6H_4$	4m	84
14	3-$CH_3C_6H_4$	4n	82

[a] Reaction conditions: 1(a–n) substituted benzaldehydes (4.71 mmol), 2 ethyl acetoacetate (9.42 mmol), 3 ammonium acetate (5.66 mmol), and 20% $AlCl_3$@ZnO (1.17 mmol) under solvent-free conditions, room temperature, 2 h. [b] Isolated yield.

turn, attacking enolate to offer more α,β-unsaturated-enone (A). Whereas another equivalent of ethyl acetoacetate may react with ammonia to form 3-aminobut-2-enoate (B). Thus, further intermediates (A) and (B) can be condensed in the presence of a catalyst to form the desired 1,4-dihydropyridine (Fig. 11). Thus, the ZnO material in the presence of $AlCl_3$ can enhance the catalytic activity by providing more catalytically active sites. Hence, the combined effect of $AlCl_3$@ZnO requires a smaller amount of catalyst in the setting of solvent-free conditions at room temperature. The proposed mechanism of reaction is shown in Fig. 11.

3.7.6. Catalyst recyclability. As discussed in the experimental section, chloroform was added to the reaction mass after completion of the reaction. The chloroform layer was separated by a simple filtration technique and pure 1,4-dihydropyridine product was obtained from it. Simultaneously, the residual solid material was washed with chloroform and ethyl alcohol and then subjected to oven drying at 120 °C for 2 h. The recovered catalyst was again reused for the same reaction three times. The results obtained for 1,4-dihydropyridine synthesis by using the reused catalyst are displayed in Table 7.

The loss of 1,4-dihydropyridine product yield after each catalytic cycle is displayed in Table 7. The decrease in yield might be due to some loss of catalyst after each cycle, which may be associated with the amorphous nature of $AlCl_3$. The durability of the proposed catalyst up to the 3rd cycle is quite good.

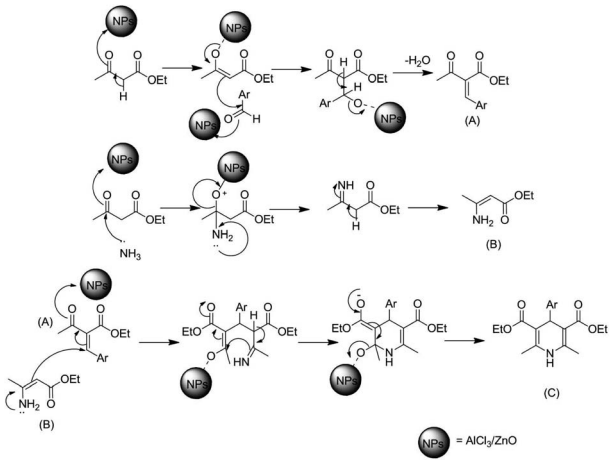

Fig. 11 Proposed mechanism for the synthesis of 1,4-dihydropyridine using $AlCl_3$@ZnO nanocatalyst.

Table 7 Recyclability study of $AlCl_3$@ZnO catalysts[a]

Run	Yield[b] (%)
1	92
2	79
3	62
4	42

[a] Reaction conditions: 1 benzaldehyde (4.71 mmol), 2 ethyl acetoacetate (9.42 mmol), 3 ammonium acetate (5.66 mmol), and 20% $AlCl_3$@ZnO under solvent-free conditions, room temperature, 2 h. [b] Isolated yield.

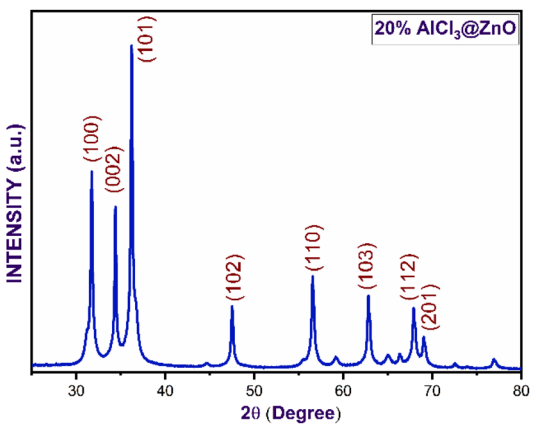

Fig. 12 XRD of recovered 20% $AlCl_3$@ZnO nanocatalyst after 4 h of drying at 120 °C.

However, the activity of the catalyst can be retained by careful washing and drying and maintaining the same reaction time. To check any structural and composition changes in the recovered catalyst, we took XRD of recovered $AlCl_3$@ZnO catalyst materials after 4 h of drying at 120 °C. The XRD of recovered catalyst material fully matches with hexagonal wurtzite phase of ZnO, which is also revealed in the XRD of fresh $AlCl_3$@ZnO catalyst. The particle size of the recovered catalyst was

© 2023 The Author(s). Published by the Royal Society of Chemistry

Open Access Article. Published on 18 Avost 2023. Downloaded on 08/12/2025 08:13:16.
This article is licensed under a Creative Commons Attribution-NonCommercial 3.0 Unported Licence.

calculated using Scherrer's equation and was found to be 32.96 nm while it is found to be 33.62 nm for the fresh catalyst (Fig. 12).

4. Conclusion

We successfully accomplished Hantzsch pyridine synthesis using nanocrystalline $AlCl_3$@ZnO nanocatalyst. The reported catalyst is highly efficient, environmentally friendly, and recyclable and could become an alternative to routine homogenous and heterogenous catalytic reactions. The required ZnO nanoparticles were prepared by a simple solution-based precipitation method. Whereas loading of $AlCl_3$ on the ZnO nanocatalyst was carried out by a wet-impregnation technique. The as-synthesized catalyst with an average particle size of 70–80 nm is found to be more effective for the synthesis of dihydropyridine derivatives. The catalyst confers 92% yield for the preparation of 1,4-dihydropyridines under solvent-free and room temperature conditions. The as-synthesized catalyst is stable and easily handled and can be used for scale–up reactions. It is reasonable for us to emphasize that the overall methodology for 1,4-dihydropyridine synthesis is economical and environmentally friendly.

Conflicts of interest

There are no conflicts to declare.

Acknowledgements

The author S. T. Shinde is very thankful to the chemistry department and Principal of Annasaheb Awate College Manchar, Pune and Director, Centre for Materials for Electronic Technology (C-MET), Pune for providing necessary facilities. The author also thanks CIF, SPPU Pune for providing the characterization facilities.

References

1 B. Gauni, K. Mehariya, A. Shah and S. M. Duggirala, *Eur. Chem. Bull.*, 2021, **10**, 21–34.
2 J. Y. Zhang and X. Q. Zhu, *Molecules*, 2022, **27**(17), 5382, DOI: 10.3390/molecules27175382.
3 V. K. Sharma and S. K. Singh, *RSC Adv.*, 2017, **7**, 2682–2732.
4 X. Yu and D. Sun, *Molecules*, 2013, **18**, 6230–6268.
5 E. Pop, B. M. E. rewster, M. J. Huang and N. Bodor, *J. Mol. Struct.: THEOCHEM*, 1995, **337**(1), 49–55.
6 P. A. Datar and P. B. Auti, *J. Saudi Chem. Soc.*, 2016, **20**(5), 510–516, DOI: 10.13140/RG.2.2.33495.37282.
7 Y. Ozawa, K. Hayashi and H. Kobori, *Curr. Hypertens. Rev.*, 2006, **2**(2), 103–111.
8 P. Olejníková, L. Švorc, D. Olšovská, A. Panáková, Z. Vihonská, K. Kovaryová and Š. Marchalín, *Sci. Pharm.*, 2014, **82**, 221–232.
9 A. M. Vijesh, A. M. Isloor, S. K. Peethambar, K. N. Shivananda, T. Arulmoli and N. A. Isloor, *Eur. J. Med. Chem.*, 2011, **46**, 5591–5597.
10 P. Olejníková, Ľ. ŠVORC, D. Olšovská, A. Panáková, Z. Vihonská, K. Kovaryová and Š. Marchalín, *Sci. Pharm.*, 2014, **82**(2), 221–232, DOI: 10.3389/fmicb.2022.874709.
11 X. F. Zhou, L. Zhang, E. Tseng, E. Scott-Ramsay, J. J. Schentag, R. A. Coburn and M. E. Morris, *Drug Metab. Dispos.*, 2005, **33**, 321–328.
12 M. A. Shaldam, M. H. Elhamamsy, E. A. Esmat and T. F. El-Moselhy, *ISRN Med. Chem.*, 2014, **2014**, 1–14.
13 D. B. Tikhonov and B. S. Zhorov, *J. Biol. Chem.*, 2009, **284**, 19006–19017.
14 R. Miri, K. Javidnia, H. Sarkarzadeh and B. Hemmateenejad, *Bioorg. Med. Chem.*, 2006, **14**, 4842–4849.
15 M. T. Jafari-Chermahini and H. Tavakol, *ChemistrySelect*, 2021, **6**, 2360–2365.
16 Y. T. Zhou, L. S. Yu, S. Zeng, Y. W. Huang, H. M. Xu and Q. Zhou, *Ther. Clin. Risk Manage.*, 2014, **10**, 17–26.
17 U. Klotz, *Arzneimittelforschung*, 2002, **52**(03), 155–161.
18 R. K. Singh, K. Sahore, R. Rana, S. Kumar and D. N. Prasad, *Iran. J. Catal.*, 2016, **6**(4), 389–408.
19 N. Deswal, A. Shrivastava, M. Summon Hossain, P. Gahlyan, R. Bawa, R. D. Gupta and R. Kumar, *ChemistrySelect*, 2021, **6**, 717–725.
20 M. Iman, A. Davood, G. Dehqani, M. Lotfinia, S. Sardari, P. Azerang and M. Amini, *Iran. J. Pharm. Res.*, 2015, **14**(4), 1067–1075.
21 N. J. A. Martin and B. List, *J. Am. Chem. Soc.*, 2006, **128**, 13368–13369.
22 S. A. Van Arman, A. J. Zimmet and I. E. Murray, *J. Org. Chem.*, 2016, **81**, 3528–3532.
23 T. He, R. Shi, Y. Gong, G. Jiang, M. Liu, S. Qian and Z. Wang, *Synlett*, 2016, **27**, 1864–1869.
24 Y. Lu, S. Wilhelm, M. Bai, P. Maness and L. Ma, *Biochemistry*, 2019, **58**, 4035–4046.
25 K. Aswin, K. Logaiya, P. N. Sudhan and S. S. Mansoor, *J. Taibah Univ. Sci.*, 2012, **6**, 1–9.
26 A. Debache, R. Boulcina, A. Belfaitah, S. Rhouati and B. Carboni, *Synlett*, 2008, **4**, 509–512.
27 A. Kumar and R. A. Maurya, *Synlett*, 2008, **6**, 883–885.
28 V. Sivamurugan, R. Suresh Kumar, M. Palanichamy and V. Murugesan, *J. Heterocycl. Chem.*, 2005, **42**, 969–974.
29 S. Das Sarma, P. Pahari, S. Hazarika, P. Hazarika, M. J. Borah and D. Konwar, *Arkivoc*, 2013, **2013**, 243–263.
30 M. R. Asghariganjeh and P. Nasirveise, *Asian J. Chem.*, 2013, **25**, 2937–2938.
31 A. Hasaninejed, M. R. Kazerooni and A. Zare, *Catal. Today*, 2012, **196**, 148–155.
32 R. Ballini, F. Bigi, M. L. Conforti, D. De Santis, R. Maggi, G. Oppici and G. Sartori, *Catal. Today*, 2000, **60**, 305–309.
33 S. T. Shinde, K. G. Kanade, B. K. Karale, D. P. Amalnerkar, N. M. Thorat, S. S. Arbuj and S. P. Kunde, *Curr. Smart Mater.*, 2016, **1**(1), 68–76, DOI: 10.2174/2405465801666160601 12.
34 S. P. Kunde, K. G. Kanade, B. K. Karale, H. N. Akolkar, P. V. Randhavane and S. T. Shinde, *Arabian J. Chem.*, 2019, **12**, 5212–5222.
35 J. Safaei-Ghomi, M. A. Ghasemzadeh and M. Mehrabi, *Sci. Iran.*, 2013, **20**, 549–554.

Open Access Article. Published on 18 Avost 2023. Downloaded on 08/12/2025 08:13:16.
This article is licensed under a Creative Commons Attribution-NonCommercial 3.0 Unported Licence.

36 S. P. Kunde, K. G. Kanade, B. K. Karale, H. N. Akolkar, S. S. Arbuj, P. V. Randhavane, S. T. Shinde, M. H. Shaikh and A. K. Kulkarni, *RSC Adv.*, 2020, **10**(45), 26995–27005.
37 S. V. H. S. Bhaskaruni, S. Maddila, W. E. van Zyl and S. B. Jonnalagadda, *Catal. Today*, 2018, **309**, 276–281.
38 S. M. Sadeghzadeh and M. A. Nasseri, *Catal. Today*, 2013, **217**, 80–85.
39 N. Hussain, P. Gogoi, M. R. Das, P. Sengupta, V. E. Fedorov, I. P. Asanov, M. N. Kozlova and S. B. Artemkina, *Appl. Catal., A*, 2017, **542**, 368–379.
40 M. G. Dehbalaei, N. Foroughifar, A. Khajeh-Amiri and H. Pasdar, *J. Chin. Chem. Soc.*, 2018, **65**(11), 1356–1369.
41 S. B. Waghmode, S. S. Arbuj and B. N. Wani, *New J. Chem.*, 2013, **37**, 2911–2916.
42 V. U. Pandit, S. S. Arbuj, Y. B. Pandit, S. D. Naik, S. B. Rane, U. P. Mulik, S. W. Gosavi and B. B. Kale, *RSC Adv.*, 2015, **5**, 10326–10331.
43 C. Manoharan, G. Pavithra, M. Bououdina, S. Dhanapandian and P. Dhamodharan, *Appl. Nanosci.*, 2016, **6**, 815–825.
44 X. Song, Y. Wu, F. Cai, D. Pan and G. Xiao, *Appl. Catal., A*, 2017, **532**, 77–85.
45 M. J. Akhtar, H. A. Alhadlaq, A. Alshamsan, M. A. Majeed Khan and M. Ahamed, *Sci. Rep.*, 2015, **5**(1), 13876.
46 A. Al Baroot, M. Alheshibri, Q. A. Drmosh, S. Akhtar, E. Kotb and K. A. Elsayed, *Arabian J. Chem.*, 2022, **15**(2), 103606, DOI: **10.1016/j.arabjc.2021.103606**.
47 M. Usman, M. Arshad, S. S. Suvanam and A. Hallén, *J. Phys. D Appl. Phys.*, 2018, **51**(10), 105111, DOI: **10.1088/1361-6463/aaa9a1**.
48 H. Zhao, C. Hu, D. Zhang, H. Liu and J. Qu, *PLoS One*, 2016, **11**(1), e0148020, DOI: **10.1371/journal.pone.0148020**.
49 E. Hosono, S. S. Fujihara and T. Kimura, *J. Mater. Chem.*, 2004, **14**, 881–886.

© 2023 The Author(s). Published by the Royal Society of Chemistry